2

THE PARAMAGNETIC RESONANCE SPECTRUM OF AMMONIUM CHROMIUM ALUM

C. F. DAVIS, JR.
M. W. P. STRANDBERG

TECHNICAL REPORT 242
DECEMBER 9, 1955

RESEARCH LABORATORY OF ELECTRONICS
MASSACHUSETTS INSTITUTE OF TECHNOLOGY
CAMBRIDGE, MASSACHUSETTS

Reprinted from THE PHYSICAL REVIEW, Vol. 105, No. 2, pp. 447–455, January 15, 1957

The Research Laboratory of Electronics is an interdepartmental laboratory of the Department of Electrical Engineering and the Department of Physics.

The research reported in this document was made possible in part by support extended the Massachusetts Institute of Technology, Research Laboratory of Electronics, jointly by the U. S. Army (Signal Corps), the U. S. Navy (Office of Naval Research), and the U. S. Air Force (Office of Scientific Research, Air Research and Development Command), under Signal Corps Contract DA36-039 SC-64637, Project 102B; Department of the Army Project 3-99-10-022; Project DA 3-99-10-000.

Reprinted from THE PHYSICAL REVIEW, Vol. 105, No. 2, 447–455, January 15, 1957
Printed in U. S. A.

Paramagnetic Resonance Spectrum of Ammonium Chromium Alum*

C. F. DAVIS, JR., AND M. W. P. STRANDBERG
Department of Physics and Research Laboratory of Electronics, Massachusetts Institute of Technology, Cambridge, Massachusetts

(Received September 11, 1956)

A detailed solution of the fine-structure splitting of the ground state of the chromium ion is given. This solution assumes an electric field of cubic symmetry with a small trigonal distortion and the residual spin-orbit coupling superposed. The effect of a magnetic field at an arbitrary orientation is calculated.

Absorption positions and relative intensities are calculated and checked with experiment. Lines of character predominantly $\Delta S_z=2$, 3 are shown to have sufficient $\Delta S_z=1$ character to give the experimentally determined intensities. So-called "forbidden transitions" are accounted for quantitatively by this detailed calculation. Shapes of absorption peaks are Lorentzian for dilute specimens and Gaussian for full-strength alum. A small variation of trigonal Stark field from one paramagnetic ion to another is sufficient to account for the observed line width.

1. INTRODUCTION

ONE of the classical problems in paramagnetic resonance is the problem of the spectrum of the chromium alums. Although these materials have been studied in great detail and much has been written about them, disagreement and somewhat spotty experimental checks mark the field. It is the purpose of this paper to show that a straightforward quantum-mechanical calculation based on accepted assumptions[1] corresponds in a gratifying way with experimental results. For example, Malvano and Panetti[2] were the first to observe some small-intensity, low-field lines. These are in positions where corresponding "forbidden transitions" might be expected to occur, and so they have often been incorrectly interpreted.

The equipment used in this work is described elsewhere.[3] It is suitable for this particular kind of experiment because it includes a cavity that can be easily and accurately oriented. The signal (derivative) obtained from a uniformly swept field is recorded continuously.

2. CRYSTALLINE STARK SPLITTING

The theory of setting up the crystalline field and of determining an effective Hamiltonian is adequately handled elsewhere.[4] However, it is well to reiterate some of the assumptions normally made. These adequately, but not uniquely, determine the experimental results outlined in Secs. 4, 5, and 6.

The paramagnetic ion (positive) is surrounded by a regular array of water molecules and negative ions. These ions, and even to a larger extent the electric dipoles of six waters of hydration (chromium's nearest neighbors), profoundly influence the energy-level pattern of the paramagnetic ion. The unpaired $3d$ electrons are practically unshielded; consequently, the (^4F) ground state is decomposed by the cubicly symmetrical electric environment of the chromium ion into a singlet (Γ_2) and two triplets (Γ_4,Γ_5). The triplets lie much higher than the singlet level, giving absorption lines in the visible region. The orbital momentum projection, L_z, is no longer diagonal, nor is it a good quantum number; it can be said to be "quenched." Thus, electron motion is "locked" into the field of its neighbors and cannot contribute to the first-order magnetism.

The optical absorption spectra of solids usually occur as fairly broad bands; however, sharp line spectra can be observed in some iron and rare earth group salts. Line abosrption is associated with paramagnetic ions and is caused by transitions of unpaired electrons of an incomplete inner shell.[5]

The electron spin is not affected by its electric environment except through the mechanism of spin-orbit coupling. As we have stated above, the influence of the cubic field leaves the space components of orbital angular momentum in the Γ_2 singlet ground level with no diagonal elements. As long as we restrict ourselves to levels coming from the ground state (^4F),[6–8] it is reasonable to expect a satisfactory representation of the spin-orbit coupling by the single-parameter form:

$$A\mathbf{L}\cdot\mathbf{S}.$$

Hence, the spin-orbit operator, lacking near-degeneracy, gives no first-order contribution.

The excited Γ_5,Γ_4 levels are further split by an electric field of symmetry lower than cubic, and the orbitally

* This work was supported in part by the Army (Signal Corps), the Air Force (Office of Scientific Research, Air Research and Development Command), and the Navy (Office of Naval Research).

[1] J. H. Van Vleck, *The Theory of Electric and Magnetic Susceptibilities* (Oxford University Press, London, 1932).

[2] R. Malvano and M. Panetti, Nuovo cimento **7**, 28 (1950).

[3] Strandberg, Tinkham, Solt, and Davis, Rev. Sci. Instr. **27**, 596 (1956).

[4] R. Schlapp and W. G. Penney, Phys. Rev. **42**, 666 (1932); P. H. E. Meijer and H. J. Gerritsen, Phys. Rev. **100**, 742 (1956).

[5] J. H. Van Vleck, Phys. Rev. **57**, 426 (1940).

[6] Two doublet levels have been observed by Spedding and Nutting[7] at about 15 000 cm^{-1} above the ground term. According to calculations of Finkelstein and Van Vleck,[8] these doublet levels should lie about 3000 cm^{-1} above the $^4F\Gamma_5$ first excited quartet level. They also demonstrate that Russell-Saunders coupling holds well for the quartet states and that calculations for the quartet states are not greatly influenced by the proximity of the doublet state.

[7] F. H. Spedding and G. C. Nutting, J. Chem. Phys. **3**, 369 (1935).

[8] R. Finkelstein and J. H. Van Vleck, J. Chem. Phys. **8**, 790 (1940).

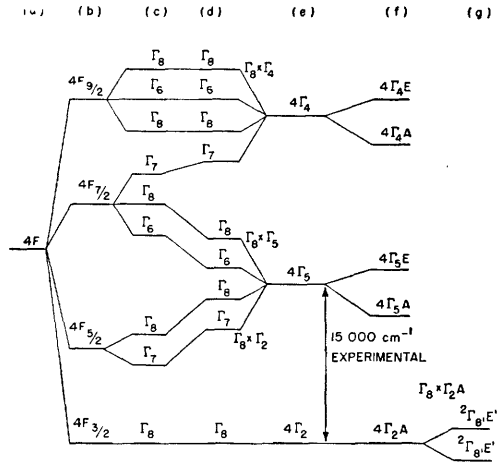

FIG. 1. Evolution of ion energy levels: (a) free ion without spin-orbit interaction; (b) free ion with spin-orbit interaction; (c) weak cubic field splitting of total angular momentum by the crystal field; (d) intermediate cubic field, including spin-orbit interaction; (e) intermediate cubic field splitting of orbital states (without spin-orbit); (f) trigonal component added; (g) spin-orbit interaction included.

singlet ground state is decomposed by the off-diagonal spin-orbit term. Kramer's theorem shows that in cases of odd half-integral spin the electric field cannot discriminate between equal spin components of opposite sign. In the chromium alums there are three unpaired electrons giving a spin fourfold-degenerate ground state. When the octahedron of water molecules[9] (the nearest neighbors of the chromium ion) is distorted slightly, the excited orbital triplets and the ground spin quartet are decomposed, the latter becoming two doublets of spin $\pm\frac{1}{2}$ and $\pm\frac{3}{2}$, respectively, and separated in energy[10] by tenths of a reciprocal centimeter. The evolution of the ion energy levels to this point is illustrated in Fig. 1.[11]

Line sharpness is dependent upon the isolation of absorbing centers and the looseness of coupling between paramagnetic electrons of different ions. To a good approximation, however, this reduces to a problem of a paramagnetic ion in the presence only of its nearest (diamagnetic) neighbors. The interaction between spins cannot be neglected entirely, since it provides one of the mechanisms for spin relaxation and accounts for the line shape.

3. SPIN HAMILTONIAN

The interaction of next smaller magnitude after the trigonal splitting and the spin-orbit coupling is the interaction of the ion with a magnetic field that may be represented as

$$\beta(g_l{}^e\mathbf{L}+g_s{}^e\mathbf{S})\cdot\mathbf{H},$$

where g is the magnetogyric factor and β is the Bohr magneton ($e\hbar/2mc$). Quadratic terms in $\mathbf{H}$ are omitted; they give rise to diamagnetism and do not contribute to the resonance results. They raise or lower all levels without changing the spacing.

Nuclear terms are very small and the resultant effects have not been observed in this work. They have been studied in samples of dilution 1:1000 by Bleaney and Bowers[12] to evaluate the nuclear spin of chromium 53.

An effective perturbing Hamiltonian can thus be written:

$$\mathcal{H}'=\beta\mathbf{H}\cdot(g_l{}^e\mathbf{L}+g_s{}^e\mathbf{S})+A\mathbf{L}\cdot\mathbf{S}.$$

As we have seen, in the ground state the $\mathbf{L}\cdot\mathbf{S}$ coupling is nondiagonal; hence it is minor, since no degeneracy with the magnitude of the constant A exists. Thus the spin and orbital states are nearly commuting systems, and it is convenient to express the perturbation term $\mathcal{H}'$ in the representation for $\mathbf{L}$, in which the energy, including the crystalline field contribution is diagonal, and in which the spin variable is a commuting system with S^2 and S_z diagonal.

Matrix elements of the first-order perturbation are

$$\begin{aligned}(S,S_z,\Gamma_2A\,|\,\mathcal{H}'\,|\,S,S_z'\Gamma_2A)&=(S,S_z\,|\,g_s{}^e\beta\mathbf{H}\cdot\mathbf{S}\,|\,S,S_z')\\&\quad+(\Gamma_2A\,|\,g_l{}^e\beta\mathbf{H}\cdot\mathbf{L}\,|\,\Gamma_2A)\\&\quad+(S,S_z\,|\,\mathbf{S}\,|\,S,S_z')\cdot(\Gamma_2A\,|\,A\mathbf{L}\,|\,\Gamma_2A).\end{aligned}$$

The energy contribution from the second-order pertubation is

$$-\sum_{\Gamma=\Gamma_5,\Gamma_4}\frac{|\,(\Gamma_2|\beta\mathbf{H}\cdot(g_l{}^e\mathbf{L}+g_s{}^e\mathbf{S})+A\mathbf{L}\cdot\mathbf{S}|\Gamma)\,|^2}{E(\Gamma)-E(\Gamma_2)},$$

where Γ_2 represents the ground state and Γ represents the excited state Γ_5,Γ_4. Since there are only orbital matrix elements between states Γ_2 and Γ, all terms not involving $\mathbf{L}$ are zero.

$$-\sum_{\Gamma}\frac{|\,(\Gamma_2|\mathbf{L}|\Gamma)\cdot(\beta g_l{}^e\mathbf{H}+A\mathbf{S})\,|^2}{E(\Gamma)-E(\Gamma_2)}.$$

The terms in H^2 are not associated with a change of transition energy within the ground state. The evaluation of the second-order (off-diagonal) contributions to the ground-state energy is essentially the first term in a contact transformation (or "Van Vleck transformation") necessary to reduce the off-diagonal term to less than second-order importance. The orbital matrix elements are constant for this ground-state calculation; hence we are left with an effective "spin-Hamiltonian." The resulting expression gives, with only the spin a variable, the properties of these off-diagonal terms of the perturbation, with the orbital dependence reduced to constant numbers that have only the function of param-

[9] H. Lipson, Proc. Roy. Soc. (London) **A151**, 347 (1935).

[10] The Jahn-Teller effect, which arises from linear vibration of the unit cell, can also supply a mechanism for degeneracy removal. However, in the chromium alums, this effect has been shown to be small compared with the effects of the cubic field. See J. H. Van Vleck, J. Chem. Phys. **7**, 72 (1939).

[11] H. Bethe, Ann. Physik Ser. 5, **3**, 133 (1929).

[12] B. Bleaney and K. D. Bowers, Proc. Phys. Soc. (London) **A64**, 1135 (1951).

eters in the problem.

$$\mathcal{H}_s'=\left[g_s{}^e\beta\mathbf{H}-A\beta g_l{}^e\sum_\Gamma\left\{\frac{(\Gamma_2|\mathbf{L}|\Gamma)\cdot\mathbf{H}(\Gamma_2|\mathbf{L}|\Gamma)}{E(\Gamma)-E(\Gamma_2)}\right\}\right]\cdot\mathbf{S}$$
$$-A^2\sum_\Gamma\frac{[\Gamma_2|\mathbf{L}|\Gamma)\cdot\mathbf{S}]^2}{E(\Gamma)-E(\Gamma_2)}.$$

The second term in the first bracket shows to what extent the spin is coupled with the orbital angular momentum. The last term together with the direct spin-spin interaction (of importance for understanding line shape, which has been ignored) describes the behavior of the spin in the absence of a magnetic field and in the presence of its atomic and crystalline surroundings. The symmetry must be the same as that of the crystalline field. Bleaney and Stevens[13] point out that this gives the "spin-Hamiltonian," and thus also the resonance spectrum, complete axial symmetry.

The magnetic field will be considered to be at an arbitrary orientation (θ,ϕ, in polar coordinates) to the crystalline *symmetry* axis. The angle θ is chosen as the polar angle, and ϕ is defined as the azimuthal angle with x at $\phi=0$. Although ϕ does not affect the line position, the intensity will be found to vary with ϕ for large θ. Thus the components of $\mathbf{H}$ are

$$H_z=H\cos\theta$$
$$H_\pm=H\sin\theta e^{\pm i\phi}.$$

To evaluate the "spin-Hamiltonian" it is necessary to recall the spin and orbital angular momentum matrix elements:

$$(k\pm1|L_\pm|k)=[l(l+1)-k(k\pm1)]^{\frac{1}{2}}=[12-k(k\pm1)]^{\frac{1}{2}},$$
$$(k|L_z|k)=k,$$
$$(m\pm1|S_\pm|m)=[S(S+1)-m(m\pm1)]^{\frac{1}{2}}=[15/4-m(m\pm1)]^{\frac{1}{2}},$$
$$(m|S_z|m)=m.$$

The unperturbed state functions for this problem are linear combinations of the free-ion solution. The only nonzero matrix elements from the ground state (Γ_2A) are shown below and their values given to the order of the trigonal field magnitude divided by that of the cubic field.

$$a^2=\frac{(\Gamma_5A|L_z|\Gamma_2A)^2}{E^0(\Gamma_5A)-E^0(\Gamma_2A)}\doteq\frac{4}{E^0(\Gamma_5A)-E^0(\Gamma_2A)},$$

$$4b^2=\frac{(\Gamma_5E^\pm|L_\pm|\Gamma_2A)^2}{E^0(\Gamma_5E^\pm)-E^0(\Gamma_2A)}\doteq\frac{8}{E^0(\Gamma_5E^\pm)-E^0(\Gamma_2A)},$$

$$4c^2=\frac{(\Gamma_4E^\pm|L_\pm|\Gamma_2A)^2}{E^0(\Gamma_4E^\pm)-E^0(\Gamma_2A)}\doteq0.$$

The $E^\pm$ states are degenerate in the absence of a magnetic field, and the magnetic field causes insignificant changes compared with their spacing from Γ_2A.

The matrix elements of the secular determinant of the spin-Hamiltonian $a_{ij}=(\mathcal{H}_{ij}-E\delta_{ij})$ are

$$a_{\pm\frac{3}{2},\pm\frac{3}{2}}=E^0(\Gamma_2A)-E\pm\tfrac{3}{2}g_s{}^e\beta H\cos\theta-a^2(g_l{}^e\beta H\cos\theta\pm\tfrac{3}{2}A)^2-(b^2+c^2)[2(g_l{}^e\beta H\sin\theta)^2+3A^2],$$
$$a_{\pm\frac{1}{2},\pm\frac{1}{2}}=E^0(\Gamma_2A)-E\pm\tfrac{1}{2}g_s{}^e\beta H\cos\theta-a^2(g_l{}^e\beta H\cos\theta\pm\tfrac{1}{2}A)^2-(b^2+c^2)[2(g_l{}^e\beta H\sin\theta)^2+7A^2],$$
$$a_{\pm\frac{1}{2},\pm\frac{3}{2}}{}^*=a_{\pm\frac{3}{2},\pm\frac{1}{2}}=\tfrac{1}{2}\sqrt{3}g_s{}^e\beta H\sin\theta e^{\mp i\phi}-2\sqrt{3}\beta g_l{}^eA(b^2+c^2)H\sin\theta e^{\mp i\phi},$$
$$a_{\pm\frac{1}{2},\mp\frac{1}{2}}=g_s{}^e\beta H\sin\theta e^{\mp i\phi}-4\beta g_l{}^eA(b^2+c^2)H\sin\theta e^{\mp i\phi}.$$

Thus the splitting of the levels with zero magnetic field is

$$(a_{\pm\frac{1}{2},\pm\frac{1}{2}}-a_{\pm\frac{3}{2},\pm\frac{3}{2}})\equiv\delta=+2a^2A^2-4A^2(b^2+c^2)\doteq\frac{8A^2E^0(\Gamma_5E)-E^0(\Gamma_5A)}{[E^0(\Gamma_5)-E^0(\Gamma_2)]^2}.$$

The effective g factor, if one considers trigonal splitting to be small compared with the cubic, is[14]

$$g=g_s{}^e-2a^2g_l{}^eA.$$

The secular determinant can be written most conveniently in terms of a normalized energy and magnetic field:

$$W=2E/\delta,\quad X=2g\beta H/\delta;$$

$$0=(\mathcal{H}-W)=\begin{bmatrix}-(W+1)-\frac{3}{2}X\cos\theta & \frac{1}{2}\sqrt{3}X\sin\theta e^{-i\phi} & 0 & 0\\ \frac{1}{2}\sqrt{3}X\sin\theta e^{+i\phi} & -(W-1)-\frac{1}{2}X\cos\theta & X\sin\theta e^{-i\phi} & 0\\ 0 & X\sin\theta e^{+i\phi} & -(W-1)+\frac{1}{2}X\cos\theta & \frac{1}{2}\sqrt{3}X\sin\theta e^{-i\phi}\\ 0 & 0 & \frac{1}{2}\sqrt{3}X\sin\theta e^{+i\phi} & -(W+1)+\frac{3}{2}X\cos\theta\end{bmatrix}.$$

The secular equation is thus

$$W^4-W^2[2+(5/2)X^2]+2X^2W(3\cos^2\theta-1)+1-3X^2\cos^2\theta+\tfrac{1}{2}X^2+(9/16)X^4=0.$$

A graph showing the energy dependence with field is shown in Fig. 2.

The spin state functions T^* can be found by solving

$$(\mathcal{H}-W)T^*=0$$

and the appropriate spin matrix elements can be obtained by multiplying the spin matrix for a particle of

[13] B. Bleaney and K. W. H. Stevens, Repts. Progr. Phys. 16, 108 (1953).

[14] W. H. Kleiner, J. Chem. Phys. 20, 1784 (1952), gives experimental and theoretical evidence that the value of the spin-orbit coupling parameter, A, is practically independent of the crystalline perturbation.

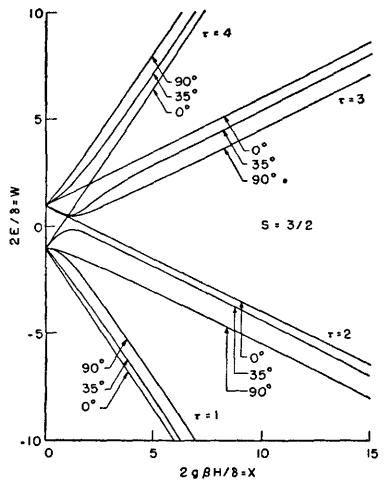

FIG. 2. Energy dependence with field.

spin $\frac{3}{2}$,

$$TS_{\pm,z}T^*,$$

with

$$(S_z)=\begin{bmatrix}-\frac{3}{2} & 0 & 0 & 0\\ 0 & -\frac{1}{2} & 0 & 0\\ 0 & 0 & +\frac{1}{2} & 0\\ 0 & 0 & 0 & +\frac{3}{2}\end{bmatrix},$$

$$(S_+)=\begin{bmatrix}0 & \sqrt{3} & 0 & 0\\ 0 & 0 & 2 & 0\\ 0 & 0 & 0 & \sqrt{3}\\ 0 & 0 & 0 & 0\end{bmatrix},$$

and (S_-) is the transpose conjugate of (S_+).

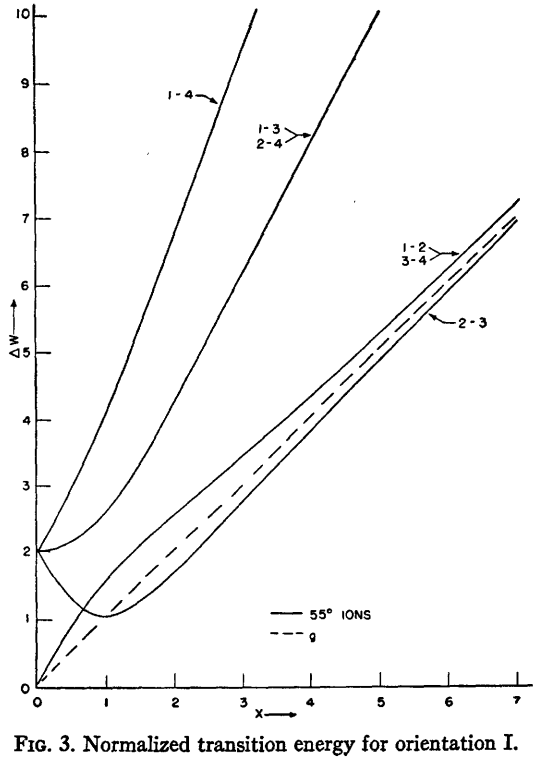

FIG. 3. Normalized transition energy for orientation I.

It is well to note that mixing of the state functions from the Γ_5,Γ_4 level is

$$T^*=T^*(\Gamma_2 A)-\sum_{\Gamma}\frac{(\Gamma|\mathbf{L}|\Gamma_2)\cdot(\beta\mathbf{H}+A\mathbf{S})}{E(\Gamma)-E(\Gamma_2)}T^*(\Gamma).$$

Since A is in the order of $100\,\mathrm{cm}^{-1}$ and the denominators of the summation are all in excess of $15\,000\ \mathrm{cm}^{-1}$, the mixing will be in the order of 1%, which is negligible as far as intensities are concerned.

The diagonal matrix elements of the TS_zT^* matrix illustrate the significance of the axial component of spin as a quantum number. These values lie fairly close to those of a free particle of spin $\frac{3}{2}$ for the $-\frac{3}{2}$ level, and also for values of θ close to zero and at high fields (Paschen-Back). For other fields and orientations the spectral notation becomes more complex, but it can still be simply represented in the correct reference scheme (see Sec. 5).

4. EXPERIMENTAL TECHNIQUES

The apparatus used is described elsewhere.[3] The magnetic field was homogeneous to better than 0.1 gauss over the specimen, and line positions were measured by a proton resonance probe and a BC 221 frequency meter. Crystals of various dilutions (with the corresponding aluminum alum) were grown and subsequently analyzed for chromium and aluminum. Dilutions were expressed as mole fraction. These crystals with faces perpendicular to (111) axes (orientation I) were ground in jigs to show a face perpendicular to a (100) axis (orientation II) and to a (110) axis (orientation III). The specimens were fastened to the rectangular cavity wall with coil cement and the cavity was positioned between the magnet pole faces by Plexiglas blocks. Monitoring of line shape and line width assured accurate orientation. Section 6 indicates that the width of the central absorption line is a very strong function of orientation.

TABLE I. Scale factors.[a]

This work	Weiss	Kittel and Luttinger	Unnormalized
X	ξ	$2\sqrt{3}x$	$2g\beta H/\delta$
ΔW	$2\Delta W/\delta$	$2\Delta\epsilon$	$2h\nu/\delta$

[a] δ is the zero-field splitting in energy units, H is the static magnetic field, and ν is the frequency of the rf field.

Lines of all diluted specimens were found to be Lorentzian. Widths were taken as the difference in field between maximum and minimum of the differential absorption curve. This width multiplied by $\partial\nu/\partial H$ gives almost a constant. A notable exception is the 3–2 lines in orientation II. Although these include four superposed lines, they are much narrower than any other lines of the spectrum. This is reasonable if we assume that some of the broadening is the result of a

TABLE II. Orientations.

Plane normal to H	θ	Orientation index: This work	Weiss	Kittel and Luttinger
(100)	55°	I	I	(001)
(111)	0°–70°	II	II	...
(110)	35°–90°	III	...	...

random distribution of trigonal Stark field (responsible for the splitting, δ) at the paramagnetic ions, as Meijer[15] postulated. The 3–2 line widths depend on δ only in high order, whereas all other lines are first order in δ.

Since field derivative curves were obtained, the total absorption could only be found by measuring the area under the curve and multiplying it by the width. It can be seen from chart 8, which gives the results of electronic integration, that it is possible to make a better approximation.

5. CALCULATED VALUES

The energy levels are designated by τ values and are numbered 1 through 4 from the lowest. This scheme permits comparison of energies and matrix elements as continuous self-consistent functions of the field, in all nondegenerate cases.

Line positions are found as the differences between roots of the secular equation. Graphs of normalized transition energy as a function of normalized field are given for various orientations of the whole crystal (Figs. 3, 4, and 5). These correspond (Tables I, II, and III) to calculations made by Weiss and by Kittel and Luttinger. All matrix elements for each transition were calculated for selected orientations and magnetic fields. An example of these matrix elements ($\tau=2\rightarrow4$) is included (Fig. 6). Note that, at $\theta=0°$ and $\theta=90°$, the $S_{\pm}$ elements are not continuous. These discontinuities result from the choice of nomenclature. At $\theta=0°$, the matrix-element discontinuities represent discontinuities in energy level slope at degeneracies. These discontinuities and degeneracies disappear at any other orientation and cancel when combined to form any observable quantity. At $\theta=90°$, the choice of orthogonal wave functions for the degenerate $\tau=1$ and 2 energy levels would result in continuity of matrix elements, but in confusion in the significance of matrix elements at other angles and fields.

TABLE III. Correlation of level identification with P. R. Weiss designation.

Level	Orientation angle θ: 0°	55°	70°
$\tau=1$	$-\frac{3}{2}$	$\pm\frac{3}{2}$	$+\frac{3}{2}$
$\tau=2$	$-\frac{1}{2}$[a]	$\pm\frac{1}{2}$	$+\frac{1}{2}$
$\tau=3$	$+\frac{1}{2}$[a]	$\mp\frac{1}{2}$	$-\frac{1}{2}$
$\tau=4$	$+\frac{3}{2}$[a]	$\mp\frac{3}{2}$	$-\frac{3}{2}$

[a] At fields greater than $X=2$.

[15] P. H. E. Meijer, Physica 17, 899 (1951).

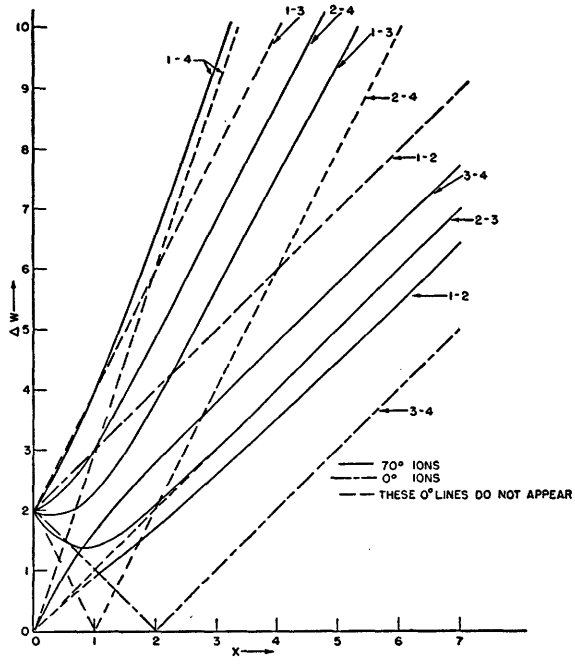

FIG. 4. Normalized transition energy for orientation II.

The theoretical values of relative line intensities were calculated as the square of the matrix element appropriate to the direction of the rf magnetic field. These values are independent of the azimuthal angle ϕ (see Fig. 7) for two crystal orientations. Since the theoretical absorption is of a line observed at constant field as a

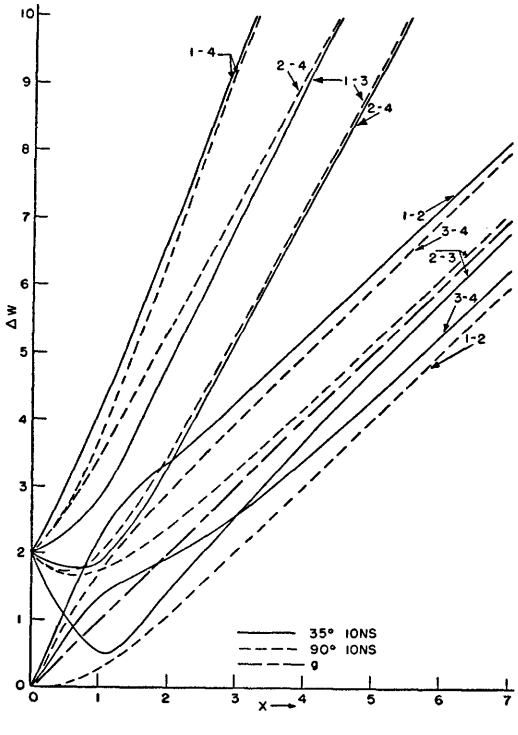

FIG. 5. Normalized transition energy for orientation III.

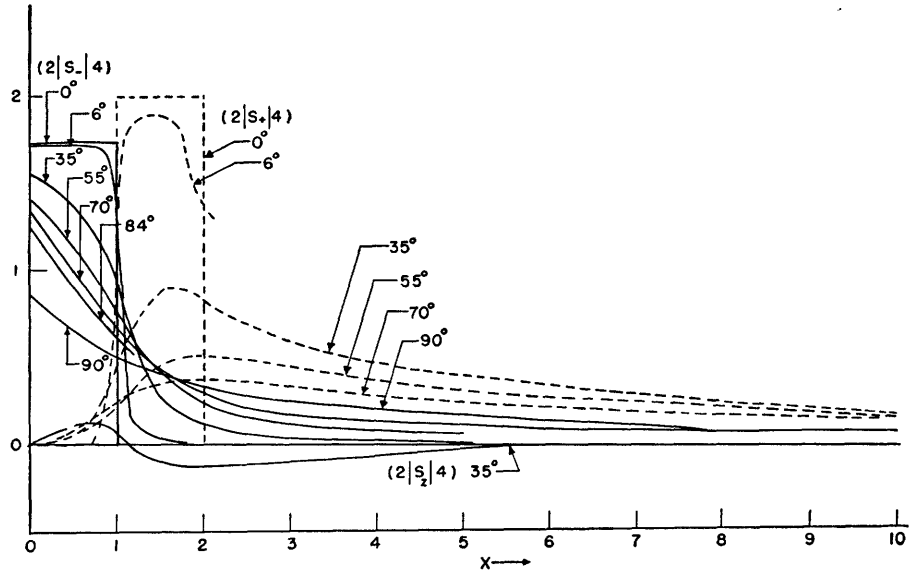

FIG. 6. $T=2\rightarrow4$ matrix elements

function of frequency, while the observations were made at constant frequency, conversion must be made. This is accomplished to a first order by the factor $h\partial\nu/\beta\partial H$, the slope of the transition energy curve as a function of magnetic field.

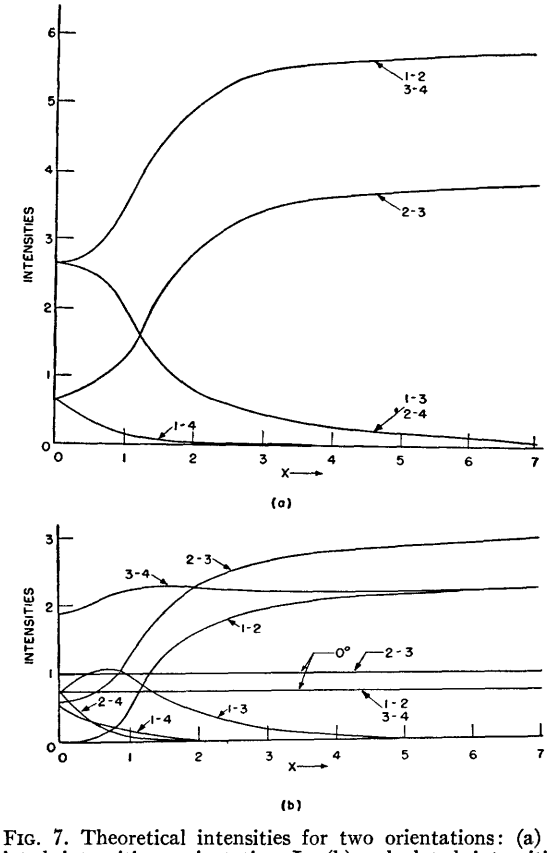

FIG. 7. Theoretical intensities for two orientations: (a) calculated intensities—orientation I; (b) calculated intensities—orientation II.

6. DERIVED RESULTS

The effective g factor, which was isotropic to experimental accuracy, was measured at several temperatures, frequencies, and dilutions. The deviation of the g factor from that of the free electron relates the spin-orbit coupling parameter A and the magnitude of the cubic field (see Table IV) as

$$g_s{}^e-g=\frac{8g_t{}^eA}{E^0(\Gamma_5A)-E^0(\Gamma_2A)}.$$

The values in Table IV were calculated from $g=h\nu/\beta H$, where H is the magnetic field of the zero-orientation 3–2 transition.

Calculation of the g factor is dependent upon finding the center of the 0° line, which is partly degenerate with the 70° lines of the 3–2 transition. For the very dilute alum at room temperature, the two are quite degenerate at K band ($\Delta H=0.085$ gauss), degenerate but interfering at X band ($\Delta H=1.40$ gauss), and distinct but not entirely separate at S band ($\Delta H=27$ gauss). Correction was made for this phenomenon at room temperature, but it was not required in the low-temperature (80°K) case, where the splitting is very small in the diluted alums. The limit of accuracy of these values is derived from the accuracy of calibration of the cavity wave

TABLE IV. Measured g factor.[a]

	Room temperature		Liquid nitrogen	Cr:Al
	Main peak	Extreme lines		
K band	1.974			1:47
X band	1.9766(corr)	1.974[b]	1.9765	1:47
S band	1.9737			1:47

[a] Probable error of g factor is 0.05%.
[b] In this case the average of the g factors for the 1–2 and 3–4 transitions.

TABLE V. Comparison of line positions and intensities.

Very dilute ammonium chrome alum
(Cr:Al = 1:47; $g = 1.975$; $\delta_{25°C} = 0.09833\ cm^{-1}$)

Description	Orientation	Transition	Theoretical $\partial W/\partial X$	Theoretical X	Theoretical H (gauss)	Theoretical Intensity	Experimental H (gauss)	Experimental Line area	Experimental Line width (gauss)	Ratio (column No.) $\frac{4\times9\times10}{7}$
	I(100)									
S band, Chart 4	55°	2–3	1.05	2.508	1323	3.29	1320	1.07	28	9.6
$\lambda = 9.315$ cm		1–2,3–4	0.88	1.642	866	4.60	866	1.61	31	9.6
$\delta = 0.09728\ cm^{-1}$		1–3,2–4	0.62	0.629	332	2.42	327	0.67	47	8.1
$H = 527.5\ X$ gauss		1–4	1.88	0.115	61	0.61	61	0.15	22	10.2
$W = 2.207$										
	I(100)									
X band, Charts 5, 6	55°	2–3	1.02	5.955	3245	3.80	3244	1.66	28	12.5
$\lambda = 3.4261$ cm		1–2,3–4	0.96	5.562	3031	5.90	3033	2.84	31	14.3
$\delta = 0.10051\ cm^{-1}$		1–3,2–4	1.95	2.832	1543	0.48	1542	0.125	27	13.7
$H = 545.0\ X$ gauss		1–4	2.64	1.656	902	0.08	900	0.012	28	11.0
$W = 5.795$										
	II(111)									
S band, Chart 1	0°	3–4	1.00	4.207	2219	0.75	2217	0.52	32	22.6
$\lambda = 9.315$ cm	70°	1–2	0.89	2.570	1356	1.88	1356	0.87	57	23.5
$\delta = 0.09728\ cm^{-1}$	0°	2–3	1.00	2.207	1164	1.00	1160	0.78	28	21.8
$H = 527.5\ X$ gauss	70°	2–3	0.90	2.154	1136	2.38	1130	2.33	28	24.6
$W = 2.207$	70°	3–4	1.11	1.434	756	2.29	758	1.40	31	21.0
	0°	1–2	1.00	0.207	109	0.75	107	0.52	40	28.0
	70°	1–3	0.98	0.903	475	1.04	471			
	70°	2–4	0.80	0.315	166	0.54	161			
	70°	1–4	1.6	0.148	78	0.47	66			
	II(111)									
X band	0°	3–4	1.00	8.950	4401	0.75	4400	1.58	26	55.0
$\delta = 0.09068\ cm^{-1}$	70°	1–2	0.98	7.529	3702	2.22	3702	2.84	38	48.0
$H = 491.7\ X$ gauss	0°	2–3	1.00	6.950	3417	1.00				
$W = 6.950$	70°	2–3	1.00	6.947	3416	2.94				
	70°	3–4	0.99	6.200	3048	2.24	3053	2.93	37	48.0
	0°	1–2	1.00	4.950	2434	0.75	2433	1.48	25	49.0
	70°	1–3	1.88	3.706	1823	0.10	1820	0.10	21	40.0
	70°	2–4	1.94	3.053	1501	0.01				
	70°	1–4	2.78	2.142	1053	0.02				
	II(111)									
X band, Chart 2	0°	3–4	1.00	7.794	4248	0.75	4248	0.36	35	16.8
$\delta = 0.10051\ cm^{-1}$	70°	1–2	0.98	6.344	3457	2.20	3459	0.54	43	10.8
$H = 545.0\ X$ gauss	0°	2–3	1.00	5.794	3158	1.00	{3155	1.88	20}	{9.6}
$W = 5.794$	70°	2–3	1.00	5.790	3156	2.93	}		}	{9.6}
	70°	3–4	0.99	5.031	2742	2.24	2746	0.54	38	9.3
	0°	1–2	1.00	3.794	2068	0.75	2069	0.32	33	14.1
	70°	1–3	1.89	3.088	1683	0.16	1687	0.03	24	9.0
	70°	2–4	1.94	2.480	1352	0.00				
	70°	1–4	2.68	1.71	932	0.04				
	II(111)									
K band	0°	3–4	1.00	18.364	9843	0.75	9843			
$\lambda = 1.236$ cm	70°	1–2	1.00	16.994	9107	2.25	9100	0.33	43	6.3
$\delta = 0.09885\ cm^{-1}$	0°	2–3	1.00	16.364	8771	1.00	{8769	1.52	16}	{6.1}
$H = 536.00\ X$ gauss	70°	2–3	1.00	16.364	8771	3.00	}		}	{6.1}
$W = 16.364$	70°	3–4	1.00	15.662	8395	2.25	8402	0.35	37	5.8
	0°	1–2	1.00	14.364	7699	0.75	7699	0.20	26	6.9
	70°	1–3	1.96	8.45	4542					
	70°	2–4	1.98	7.80	4189					
	70°	1–4	2.90	5.39	2885					
	III(110)									
S band, Chart 7	90°	1–2	0.98	3.170	1667	1.13	1669	0.60	33	17.0
$\lambda = 9.315$ cm	35°	2–3	1.18	2.671	1405	1.55	1403	0.76	20	12.0
$\delta = 0.09728\ cm^{-1}$	35°	3–4	0.66	2.465	1297	1.42	1301	0.18	61	5.0
$H = 526.0\ X$ gauss	90°	2–3	0.75	1.774	933	0.78	936	1.03	26	26.0
$W = 2.207$	90°	3–4	1.18	1.373	772	0.48	720	0.65	25	
	35°	2–4	1.36	1.308	688	0.21				
	90°	1–3	1.04	1.200	631	0.53				
	35°	1–2	1.96	0.961	505	0.24				
	35°	1–3	0.68	0.336	177	1.23	171	0.33	46	8.0
	90°	2–4	1.20	0.183	96	0.55	{90	0.09	23}	{5.0}
	90°	1–4	1.23	0.181	95	0.00	}		}	{5.0}
	35°	1–4	1.98	0.104	55	0.26	51	0.06	18	8.0

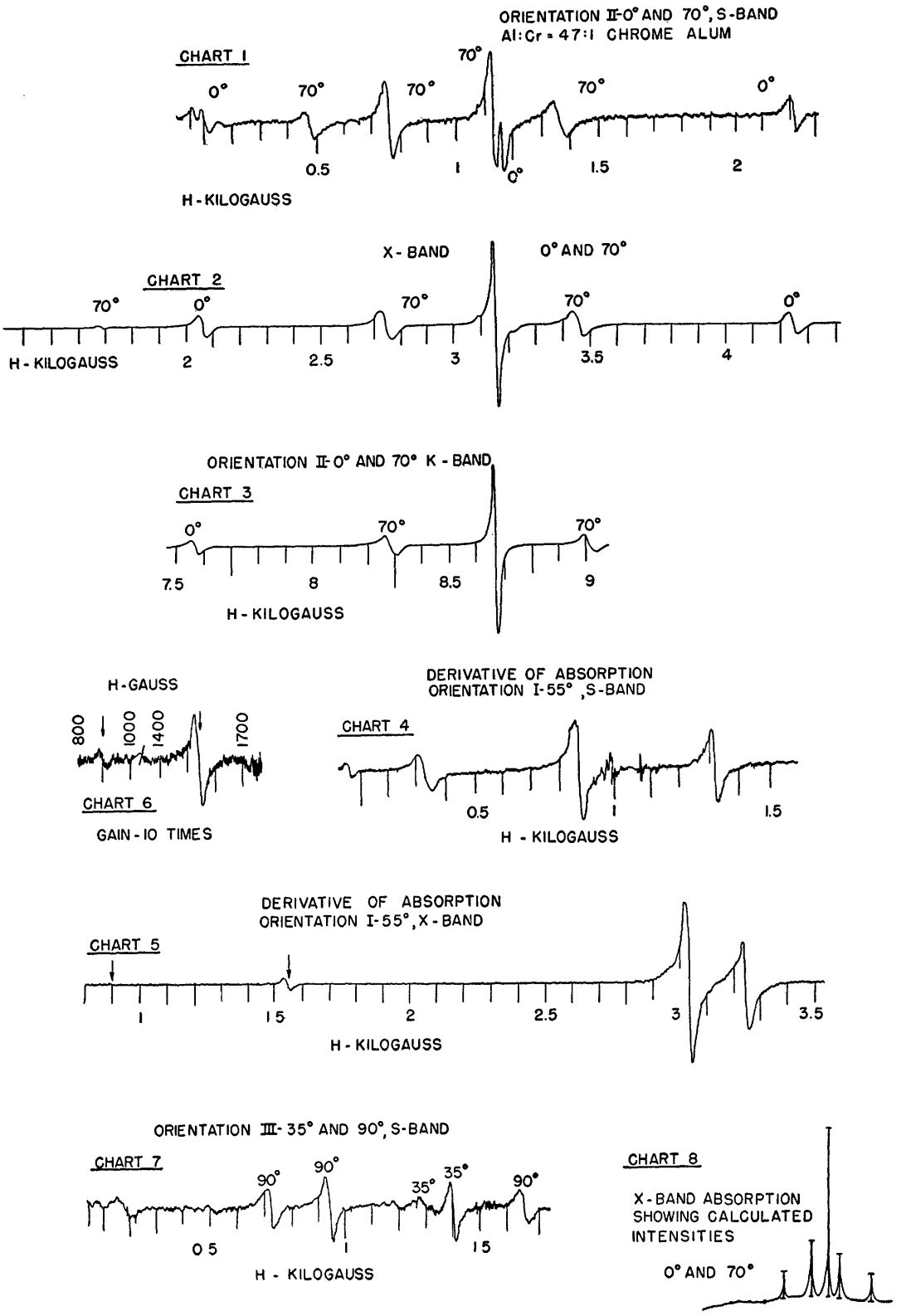

FIG. 8. Tracings of experimental charts.

TABLE VI. Measured g factors at various dilutions.

g	Cr:Al
1.9772	1:47
1.9771	1:17
1.988	1:0

TABLE VII. Zero-field splittings at 25°C.

δ	Cr:Al
0.135 $\pm$0.002 cm^{-1}	1:0
0.0984$\pm$0.001 cm^{-1}	1:17
0.0980$\pm$0.001 cm^{-1}	1:47

meter and, in the case of the g calculated from extreme lines, the temperature constancy between the two readings, since these two lines are strongly temperature dependent.

Misorientation is not a large problem, although 5° at X band would move the 70° (3–2) lines by almost 15 gauss. Since they are moved in opposite directions, observation of the main peak line width indicates whether or not this has happened; the center of gravity of these lines remains in a constant position to a first approximation (see Table V).

Charts giving the experimental data are shown as Fig. 8. These data are compared with theory in Table V. Charts 1, 2, and 3 give a comparison of the 1 to 47 dilute alum at three distinct frequencies in orientation II. The zero-degree lines maintain their relative positions and amplitudes, but the 70° lines are shown to shift and change amplitude in the lower frequency case. The 1680-gauss line at X band becomes the 470-gauss line at S band. Charts 4, 5, and 6 illustrate the same changes in going from X band to S band. Chart 6 is the portion of chart 5 that shows the two low-intensity lines with a ten times greater instrument gain. At lower frequencies it is seen that these partly forbidden lines attain much greater amplitude.

The value of the g factor is constant within experimental error throughout the temperature range (80°K to 300°K). For the other specimens, see Table VI. Whitmer, Weidner, Hsiang, and Weiss[16] give the g value of 1.99 for the undiluted alum and 1.97 for the alum diluted 1:8.5.

The zero-field splitting, δ, depends theoretically upon the deviation of the g-factor from that of the free electron and on the trigonal distortion. This is highly temperature-dependent and accounts for a large part of variation in δ. From experiment, this splitting was calculated as $g\beta\Delta H$, where ΔH is the separation in the zero-orientation spectrum of the main peak (3–2) from either of its extreme satellites (2–1, 4–3). For small deviations, θ, of the crystal from correct orientation, the calculated δ will be $(1-\frac{3}{2}\sin^2\theta)$ of the correct zero-field splitting.

Zero-field splittings at 25°C were measured as indicated in Table VII. They decrease at the rate of about 0.0005 cm^{-1}/°K to 80°K. These figures indicate a decreased trigonal distortion in the aluminum lattice at lower temperatures.

Line shape is determined by the distribution of environments of the paramagnetic centers. The environmental interactions are normally assumed to be of a dipolar type.[17] Kittel and Abrahams have calculated,[18] by the method of Van Vleck, second and fourth moments of lines as a function of dilution. They conclude that, for a random distribution of nonparamagnetic ions on the normally paramagnetic centers, a Gaussian line shape should be obtained for paramagnetic concentrations above 10% and a Lorentizan shape should be obtained for a concentration of less than 1%. In all diluted specimens of this study (paramagnetic concentration 6% and less) the shapes of all isolated lines corresponded, within less than noise, to a Lorentzian shape, but not to a Gaussian, within the same criterion.

Line width is somewhat better accounted for than line intensity by combination of two effects. Line width multiplied by $\partial\nu/\partial H$ gives almost a constant. A notable exception is found in the 3–2 lines in orientation II. Although these include four superposed lines, they are much narrower than the other lines of the spectrum. This is reasonable if we assume that some of the line broadening is caused by a random distribution of trigonal Stark fields at the paramagnetic ions, as postulated by Meijer.[15] The 3–2 lines in orientation II depend upon δ only in very high order, whereas all other lines are first order in δ.

The theory of the Stark and Zeeman splitting of the ground state of the trivalant chromium ion was considered in order to illustrate the assumptions involved. Experimental results on line positions were found to check the theory to 0.2% for the high-intensity lines and to 1% for weak lines. Relative line intensities checked with theory within a factor of two and for the simpler spectra within 20%. Line widths and line shapes correspond well to the theories of Meijer and Kittel. The identification of low-field lines seems to be confirmed. They are mainly of $\Delta S_z=2$, 3 character (which are zero intensity transitions), although they have sufficient $\Delta S_z=1$ character to give the observed intensities.

[16] Whitmer, Weidner, Hsiang, and Weiss, Phys. Rev. 74, 1478 (1948).

[17] J. H. Van Vleck, Phys. Rev. 74, 1168 (1946).

[18] C. Kittel and E. Abrahams, Phys. Rev. 90, 238 (1953).